RSC Advances

PAPER

View Article Online
View Journal | View Issue

Cite this: *RSC Adv.*, 2020, **10**, 34413

On single-electron magnesium bonding formation and the effect of methyl substitution†

Dan Yu,[a] Di Wu,[a] Jing-Yao Liu,[a] Si-Yi Li[b] and Ying Li*[a]

Received 30th July 2020
Accepted 8th September 2020

DOI: 10.1039/d0ra06591a

rsc.li/rsc-advances

The complexes formed between MgX_2 (X = F, H) molecules and alkyl radicals Y [Y = CH_3, CH_2CH_3, $CH(CH_3)_2$, and $C(CH_3)_3$] have been characterized by using quantum chemical methods. The binding distance in all cases is less than the sum of vdW radii of Mg and C, indicating the formation of a non-covalent interaction, namely single-electron magnesium bond. Energy decomposition analysis reveals that electrostatic and polarization contributions are the major components responsible for the stability of the studied complexes. According to interaction energy, atoms in molecules, and independent gradient model analyses, methyl substitution on electron donor Y imposes a positive effect on its complexation with MgX_2. When compared with other nonbonded interactions, the single-electron magnesium bond is found to have strength comparable to those of the single-electron beryllium bond and π-magnesium bond.

1. Introduction

Weak interactions, different from traditional chemical bonds, are much weaker and have longer interaction distance than corresponding covalent bonds. Nevertheless, they are no less important and play crucial roles in chemical and biochemical research[1–5] including molecular recognition,[6,7] molecular medicine,[8] functional materials design,[9] catalysis,[10] *etc.* Besides, weak interactions such as van der Waals forces, hydrogen bonding, π–π stacking effect, *etc.*, are of great significance in the formation of supramolecular systems.[11] In recent work, halogen bonding has been used as an efficient tool to control the emission color of bimetallic sliver-gold structures.[12] Lieffrig and co-workers reported the supramolecular self-assembled isostructural crystalline salts PT(1)X (X = Cl, Br) which are formed through halogen bonding interactions.[13] Weak interactions were also proved to play a part in transporting K^+ cations across lipid bilayer membranes.[14] In addition, it has been found that the cooperative effects of multiple weak interactions help to reinforce each other.[15–17] The extensive applications of weak interactions have been invoking a growing number of related research studies, which not only put forward various new forms of intermolecular or intramolecular interactions, but aid in understanding their origins.[18–20]

Hydrogen bonding is one of the most common weak interactions and was first proposed in early 20th century, and is still an active topic of scientific research due to its importance in many chemical and biological processes.[21,22] In general, a hydrogen bond has the form of X–H···Y, where the Y moiety interacts with the proton donor through its lone pair(s). Hydrogen bond interaction has an intrinsic directionality, and is characterized by saturability. In recent years, many different types of untraditional hydrogen bonds have been developed by involving diverse electron donors including conjugated molecules, radicals, metal hydrides, and even a localized electron. Correspondingly, the concepts of π-hydrogen bond,[23,24] single-electron hydrogen bond,[25] dihydrogen bond,[26] and electron hydrogen bond[27,28] have been raised successively.

Owing to the electronic similarity among lithium, sodium, and hydrogen elements, efforts have also been devoted to exploring the possibility that lithium or sodium salt molecules serve as Lewis acids to interact with electron donors. Consequently, the existence of lithium bonding[29–31] and sodium bonding[32,33] interactions has been put forward. In 2009, Yáñez and co-workers further enriched the study of non-covalent interactions with a series of beryllium bonding systems in which the BeX_2 (X = H, F, Cl, OH) molecules take the role of electron acceptor.[34] As an analog of beryllium bonds, magnesium bond was theoretically predicted shortly afterwards.[35,36] Different from beryllium and its compounds, the magnesium-containing complexes are non-toxic, which renders their experimental identification much more practicable. Besides, magnesium is an indispensable element in all the organisms and takes part in many important biochemical processes.[37,38] Thus, the in-depth study of all sorts of magnesium bonding systems may provide meaningful references for biological and environmental chemistry studies.

In the present work, we aim to gain a fundamental understanding of the interaction between magnesium salt molecules

[a]*Institute of Theoretical Chemistry, Laboratory of Theoretical and Computational Chemistry, College of Chemistry, Jilin University, Changchun 130023, P. R. China. E-mail: liyingedu@jlu.edu.cn*

[b]*Department of Transdisciplinary Science and Engineering, Tokyo Institute of Technology, 2-12-1 Ookayama, Meguro, Tokyo 152-8551, Japan*

† Electronic supplementary information (ESI) available. See DOI: 10.1039/d0ra06591a

and free radicals since the latter are known to play a crucial role in chemistry, especially organic chemistry,[39,40] atmospheric chemistry[41,42] and biochemistry.[43,44] By using quantum chemical calculations, the formation of single-electron magnesium bond between MgX_2 (X = F, H) and a series of alkyl radicals (methyl, ethyl, isopropyl, and tertiary butyl) was characterized in detail and compared with other noncovalent interactions. Besides, methyl substitution effect on structure and bonding of the resulting complexes was analyzed as well.

2. Computational details

The geometries of the $X_2Mg\cdots Y$ [X = F, H; Y = CH_3, CH_2CH_3, $CH(CH_3)_2$, and $C(CH_3)_3$] complexes and involved monomers were optimized at the MP2/aug-*cc*-pVTZ level with using the counterpoise procedure.[45] Harmonic vibrational frequency analysis was performed at the same level to affirm that these structures are local minima on their respective potential energy surfaces. Natural bond orbital (NBO) analysis[46] was performed at the MP2 level to examine the charge transfer between MgX_2 (X = F, H) and the alkyl radicals. In this work, the $\langle S^2\rangle$ values are 0.7501 for all the open-shell calculations, indicating negligible spin contamination. The above calculations were carried out by using the GAUSSIAN 09 program.[47]

The Bader's quantum theory of atoms-in-molecules (QTAIM)[48,49] was carried out to characterize the chemical bonding of the studied complexes. By the aid of Multiwfn program,[50] the bond critical points (BCPs) were found through the analysis of wave function.[51] Meanwhile, the electron density $\rho(r)$ and its corresponding Laplacian ($\nabla^2\rho$) at the BCPs were obtained. To intuitively show the studied single-electron magnesium bond in real space, we applied the independent gradient model (IGM) method[52] (embedded in the Multiwfn program) in combination with the visual molecular dynamics (VMD) program.[53] With basis set superposition error (BSSE)[54] correction, intermolecular interaction energies of the $X_2Mg\cdots Y$ complexes were obtained at the CCSD(T)//MP2/aug-*cc*-pVTZ level. To provide more insight into on the nature of interaction between MgX_2 and radical molecules, the localized molecular orbital energy decomposition analysis (LMOEDA)[55] were performed by using the GAMESS program package.[56] According to LMOEDA, the total interaction energy of a complex is composed of electrostatic (ΔE_{elstat}), exchange-repulsion (ΔE_{ex+rep}), polarization (ΔE_{pol}), and correlation (ΔE_{disp}) contributions, as shown in eqn (1)

$$\Delta E_{int} = \Delta E_{elstat} + \Delta E_{ex+rep} + \Delta E_{pol} + \Delta E_{disp} \quad (1)$$

In this work, the first three components were computed at the SCF level while the ΔE_{disp} term was obtained at the MP2 level.

3. Results and discussion

3.1 Geometric structures and single-electron magnesium bonds

The optimized structures of the $X_2Mg\cdots Y$ [X = F, H; Y = CH_3, CH_2CH_3, $CH(CH_3)_2$, and $C(CH_3)_3$] complexes are shown in Fig. 1, and the important geometrical parameters are presented in Table 1. For comparison, the geometrical structures of corresponding monomers are presented in ESI (Fig. S1†). The NPA

Table 1 Optimized geometrical parameters of the $X_2Mg\cdots Y$ [X = F, H; Y = CH_3, CH_2CH_3, $CH(CH_3)_2$, $C(CH_3)_3$] complexes at the MP2/aug-*cc*-pVTZ level. *L* and α represent the Mg$\cdots$C1 distance and the X–Mg–X angle, respectively. Bond lengths in Å and bond angles in degrees (the Mg–F bond length is 1.768 Å for the MgF_2 monomer. The Mg–H bond length is 1.706 Å for the MgH_2 monomer)

Complex	Symmetry	*L*	α	R_{Mg-X1}	R_{Mg-X2}	$D_{X1-Mg-C1-H1}$
I	C_s	2.573	163.0	1.778	1.779	0.0
II-1	C_s	2.509	160.1	1.781	1.781	32.2
II-2	C_1	2.521	160.1	1.780	1.783	12.3
III-1	C_1	2.485	158.3	1.782	1.785	28.0
III-2	C_s	2.498	157.8	1.783	1.783	89.1
IV	C_s	2.478	156.7	1.785	1.785	
I′	C_s	2.707	166.6	1.717	1.717	89.9
II′	C_s	2.644	164.3	1.719	1.719	31.8
III′	C_1	2.615	163.0	1.720	1.722	24.9
IV′	C_1	2.623	161.5	1.722	1.722	

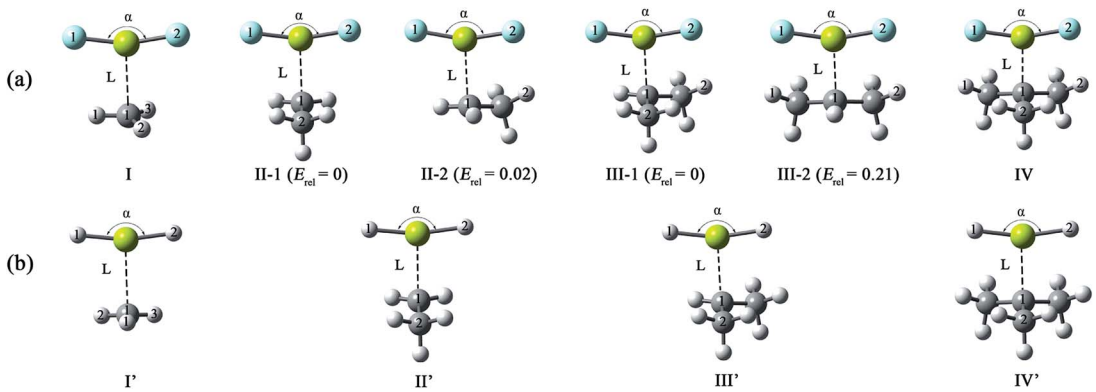

Fig. 1 Optimized structures of the (a) $F_2Mg\cdots Y$ and (b) $H_2Mg\cdots Y$ [Y = CH_3, CH_2CH_3, $CH(CH_3)_2$, $C(CH_3)_3$] complexes and the relative energies of isomers (E_{rel}, in kcal mol^{-1}) at the MP2/aug-*cc*-pVTZ level.

Table 2 NPA charges for the $X_2Mg\cdots Y$ [X = F, H; Y= CH_3, CH_2CH_3, $CH(CH_3)_2$, $C(CH_3)_3$] complexes at the MP2/aug-*cc*-pVTZ level (NPA charges are 1.863|e| and 0.932|e| for Mg and F atoms, respectively, in the MgF_2 monomer. NPA charges are 1.428|e| and −0.714|e| for Mg and H atoms, respectively, in the MgH_2 monomer)

	C1			Mg		
Complex	In monomer	In complex	Radical in complex	In complex	Δq	X1/X2 in complex
I	−0.467	−0.527	0.019	1.842	−0.021	−0.931
II-1	−0.260	−0.344	0.019	1.832	−0.031	−0.926
II-2		−0.347	0.018	1.841	−0.022	−0.931/−0.930
III-1	−0.072	−0.165	0.015	1.835	−0.028	−0.926/−0.925
III-2		−0.166	0.018	1.833	−0.030	−0.925
IV	0.102	0.011	0.004	1.844	−0.019	−0.924
I′	−0.467	−0.510	0.011	1.425	−0.003	−0.717
II′	−0.260	−0.323	0.011	1.429	0.001	−0.720
III′	−0.072	−0.140	0.012	1.433	0.005	−0.720/−0.723
IV′	0.102	0.046	0.003	1.439	0.011	−0.721

charges of the complexes and monomers are collected in Table 2.

From Fig. 1 and Table 1, both $F_2Mg\cdots CH_3$ (**I**) and $H_2Mg\cdots CH_3$ (**I′**) complexes possess C_s symmetry. Their structural difference mainly comes from different interaction orientation between X_2Mg molecule and methyl, which is reflected in the ∠X1MgC1H1 dihedral angle (0° for **I** and 89.9° for **I′**). The binding distances (L), defined as the distance between Mg and C1 atoms, are 2.573 and 2.707 Å for **I** and **I′**, respectively. The interaction between F_2Mg and ethyl, isopropyl, and tertiary butyl results in five complexes. The **II-1** and **II-2** complexes can be regarded as being obtained when the H2 and H3 atoms of $F_2Mg\cdots CH_3$ are replaced by methyl, respectively. The energy difference between them is only 0.02 kcal mol^{-1}. Similarly, the **III-1** and **III-2** isomers can be obtained when two of the methyl hydrogen atoms in $F_2Mg\cdots CH_3$ are substituted. **III-2** is 0.21 kcal mol^{-1} higher in total energy relative to **III-1**. The situation is somewhat different for the BeH_2-based system. From Fig. 1, MgH_2 binding with ethyl (or isopropyl) leads to only one structure. It can be seen that isomer **II′** resembles **II-1** in geometry, while the structure of **III′** parallels that of **III-1**. The $F_2Mg\cdots C(CH_3)_3$ (**IV**) and $H_2Mg\cdots C(CH_3)_3$ (**IV′**) complexes share a similar geometry, and the ∠F1MgC1C2 dihedral angle of 88.5° is close to the ∠H1MgC1C2 dihedral angle of 88.9°.

Besides, to evaluate the performance of modern DFT functionals for characterizing such magnesium-bonding system, structure optimizations of the $X_2Mg\cdots CH_3$ and $X_2Mg\cdots CH_2CH_3$ complexes were also performed by using the wB97XD, M06-2X, B3LYP-D3(BJ), and B2LYPD3 methods with the aug-*cc*-pVTZ basis set. The results are compared with those of the MP2 method in Table S1 in ESI.† It can be found that all these DFT functionals tend to underestimate the Mg⋯C binding distance (by 0.034–0.156 Å). For the MgF_2-based system, the wB97XD and M06-2X functionals overestimate the F–Mg–C angle while the other two underestimate it. For the MgH_2-based system, the H–Mg–C angle is always underestimated by these functionals. It is worth noting that the wB97XD and M06-2X functionals can only yield the **II-1** isomer, but fail to predict the **II-2** isomer. In contrast, the B3LYP-D3(BJ) and B2LYPD3 functionals are able to predict both structures. Hence, it can be concluded that the B3LYP-D3(BJ) and B2LYPD3 methods can be used to describe the structures of the studied species and yield basically consistent results with those obtained at the MP2 level.

From Table 1, the binding distances of the studied $X_2Mg\cdots Y$ species vary in the range of 2.478–2.707 Å, which are far shorter than 3.9 Å, namely the sum of van der Waals radii of Mg and C atoms.[57] This fact indicates a certain interaction between MgF2/MgH2 and the radicals. To illustrate this, the potential energy surfaces of the $F_2Mg\cdots CH_3$ and $H_2Mg\cdots CH_3$ complexes have been roughly obtained by scanning the Mg⋯C distance and the X–Mg–C (X = F, H) angle at the MP2/aug-*cc*-pVTZ level (see Fig. S2†). Herein, the Mg⋯C distance varies from 5.0 Å to 2.0 Å in steps of −0.3 Å, and the X–Mg–C angle increases from 90° to 102° with increments of 1.2°. As can be seen from the PES plot, the total energies of both dimers decrease as the MgX_2 molecule approaches the methyl radical, showing an attraction interaction between two species. Ultimately, minimum potential energy structures have been reached, which are basically consistent with the optimized structures of complexes **I** and **I′**. The singly occupied molecular orbitals (SOMOs) of the complexes and their corresponding free radicals are shown in

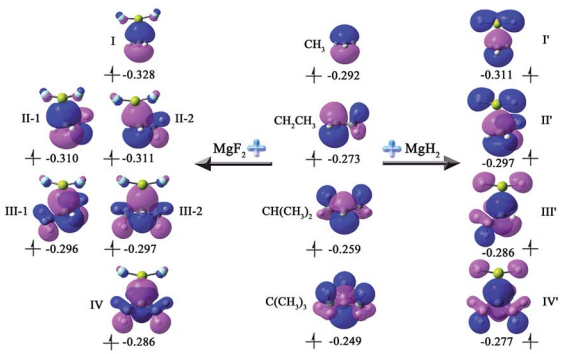

Fig. 2 The singly occupied molecular orbitals and corresponding orbital energies (in eV) of the single-electron magnesium bonding complexes and corresponding monomers at the MP2/aug-*cc*-pVTZ level.

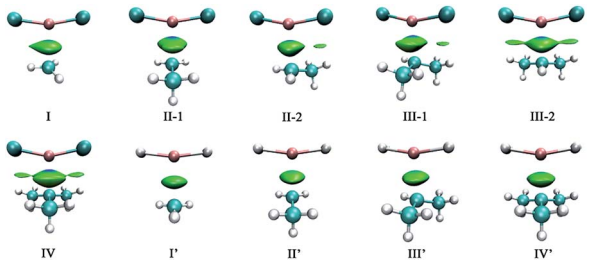

Fig. 3 The isosurfaces of δg^{inter} (isovalue = 0.01) for the $X_2Mg\cdots Y$ [X = F, H; Y = CH_3, CH_2CH_3, $CH(CH_3)_2$, $C(CH_3)_3$] complexes.

Fig. 2, where the orbital energies are also included. It can be seen that the SOMOs of complexes are mainly contributed from those of radicals, and the MgX_2 molecule acts as the single electron acceptor. Thereby the interaction between the two monomers of the $X_2Mg\cdots Y$ complexes can be defined as a single-electron magnesium bond. Furthermore, the SOMO orbital energies of complexes are lower by 0.019–0.038 eV compared with corresponding free radicals, revealing that the formation of single-electron Mg bond enhances the stability of the radicals.

To intuitively show the bonding between MgX_2 molecule and Y radicals, the independent gradient model (IGM) analysis of the $X_2Mg\cdots Y$ complexes was performed. A descriptor (δg^{inter}) is then derived that uniquely defines intermolecular interaction regions. The resulting δg^{inter} isosurfaces are presented in Fig. 3. It is known that the blue and green colors on the isosurfaces stand for strong intermolecular attractive interaction and weak van der Waals interaction, respectively. As shown in Fig. 3, the single-electron Mg bond, which mainly lies between Mg and C1 atoms, is represented by blue-green isosurfaces. Note that there are also small green regions between F of MgF_2 and methyl H atom of the radicals in the **II-2**, **III-1**, **III-2** and **IV** complexes, reflecting a weak intermolecular attraction. This can be understood given the relatively shorter F⋯H2 distances (2.706–2.762 Å) in these four dimers and the negative charge of the F atom (0.924–0.931|*e*|). The overall size of the isosurface increases as the number of methyl substituents increases, implying an increasing bonding strength. Note that the isosurfaces have more blue component for the $F_2Mg\cdots Y$ complexes compared with the H_2Mg-based series, indicating that the bonding strength of the former is stronger than that of the latter. This is consistent with the shorter *L* values of the former (2.478–2.573 Å) than those of the latter (2.623–2.707 Å).

From Table 1, the binding distance decreases in the sequence $F_2Mg\cdots CH_3$ (2.573 Å) > $F_2Mg\cdots CH_2CH_3$ (2.509 and 2.521 Å for **II-1** and **II-2**, respectively) > $F_2Mg\cdots CH(CH_3)_2$ (2.485 and 2.498 Å for **III-1** and **III-2**, respectively) > $F_2Mg\cdots C(CH_3)_3$ (2.478 Å). Hence, the methyl substitution effect on the formation of single-electron Mg bond is positive. Similarly, the Mg⋯C1 distance of the H_2Mg-based series varies in the order $H_2Mg\cdots CH_3$ (2.707 Å) > $H_2Mg\cdots CH_2CH_3$ (2.644 Å) > $H_2Mg\cdots CH(CH_3)_2$ (2.615 Å). Compared with $H_2Mg\cdots CH(CH_3)_2$, the $H_2Mg\cdots C(CH_3)_3$ complex has a slightly longer binding distance of 2.623 Å, which can be attributed to steric-hindrance effect. The case is similar to previously reported results of single-electron Be bonding systems.[58] Note that the Mg–X bond of MgX_2 is elongated by 0.010–0.017 Å upon the interaction with the Y radicals. Hence, the formation of single-electron Mg bond renders the Mg–X bonds weakened. In addition, the MgX_2 subunit bends from the linear geometry, and the bending angles (α) are 156.7–166.6° (see Fig. 1 and Table 1). From Table 1, the more methyl groups the Y radical contains, the more the MgX_2 molecule is bent.

From natural population analysis (NPA), the Y moieties carry 0.003–0.019|*e*| positive charges in the complexes (see Table 2), confirming that the radical plays the role of electron donor and MgX_2 serves as electron acceptor during the formation of single-electron Mg bond. To shed more light on the charge transfer interaction between MgF_2/MgH_2 and Y radicals, the related orbitals and corresponding second-order stabilization energies are listed in Table 3. For the F_2Mg-based series, the main charge transfer arises from the unpaired electron of C1 atom (LP(C)) to the empty 3s orbital (s*(Mg)) of Mg. For the $F_2Mg\cdots C(CH_3)_3$ complex, there is an additional electron donation from LP(C) to the empty 3p orbital of Mg. As for the H_2Mg-based complexes, the LP(C) → p*(Mg) orbital interaction is dominant in intermolecular charge transfer. Besides, there are some minor charge transfer contributions, for example, from LP(C) to σ^*_{MgH}

Table 3 Second order stabilization energies (kcal mol^{-1}) of the orbital interactions in the $X_2Mg\cdots Y$ [X = F, H, O; Y = CH_3, CH_2CH_3, $CH(CH_3)_2$, $C(CH_3)_3$] complexes

	LP(C) → s*(Mg)	LP(C) → p*(Mg)	LP(C) → σ^*_{MgH}	σ_{CH1} → p*(Mg)	σ_{CH2} → s*(Mg)	σ_{CH3} → p*(Mg)	σ_{CC} → p*(Mg)
I	20.11						
II-1	9.34						
II-2	19.08						
III-1	13.82						
III-2	9.30						
IV	9.36	2.49					
I'		14.37	2.47/2.47	1.21	1.06	1.06	
II'		13.82	2.33/2.33	1.38	1.38		
III'		11.69	2.46/1.99	1.76			
IV'		8.88	1.90/1.90				1.18

antibonding orbital, from σ_{CH} bonding orbital to the empty 3s and 3p orbitals of Mg, and from the σ_{CC} bonding orbital to p*(Mg) orbital (only for the **IV′** complex).

3.2 Interaction energies

Table 4 shows the interaction energies (E_{int}) of the studied single-electron magnesium bonding complexes. Clearly, basis set superposition error (BSSE) is not ignorable for interaction energy calculations. From the table, the BSSE values are 0.5–1.51 kcal mol^{-1} and 0.19–0.52 kcal mol^{-1} for the MgF_2- and MgH_2-based complexes, respectively. Besides, the BSSE values increase as the number of methyl groups in the radical increases and account for 9.7% and 5.5% of the CCSD(T) interaction energy for the $MgF_2\cdots C(CH_3)_3$ and $MgH_2\cdots C(CH_3)_3$ complexes, respectively. The MP2 interaction energies show a similar trend and close values to the CCSD(T) results, and their difference is less than 6.1%. Thus, the MP2 method is also reliable in calculating single-electron magnesium bonding energies. The HF method, on the other hand, is not so satisfying in interaction energy prediction, especially when it comes to the $MgH_2\cdots Y$ series. From Table 4, the electron correlation contribution contributes 14.8–27.0% and 48.4–57.6% to the CCSD(T) interaction energies of the MgF_2- and MgH_2-based complexes, respectively. From the previous reports, the electron correlation contributes 5.2%, 43.7% and 81.6% to the interaction energies of single-electron lithium bonding $H_3C\cdots LiH$,[29] single-electron hydrogen bonding $H_3C\cdots HF$[25] and single-electron beryllium bonding $H_3C\cdots BeH_2$ (ref. 58) complexes, respectively. Hence, the electron correlation contribution to single-electron magnesium bonds is comparable to that to single-electron hydrogen bonds.

With a lower-lying LUMO orbital, MgF_2 presents a higher acidity than MgH_2 molecule. Thus, a stronger interaction can be expected when the former serves as electron acceptor instead of the latter. From Table 4 and Fig. S3a,† the interaction energy of a $F_2Mg\cdots Y$ complex is 3.36–6.01 kcal mol^{-1} larger than that of corresponding $H_2Mg\cdots Y$ complex. In addition, the absolute interaction energies of the MgF_2-containing complexes follow the order $F_2Mg\cdots CH_3$ (8.61 kcal mol^{-1}) < $F_2Mg\cdots CH_2CH_3$ (11.52 and 11.70 kcal mol^{-1} for **II-1** and **II-2**, respectively) < $F_2Mg\cdots CH(CH_3)_2$ (13.81 and 14.06 kcal mol^{-1} for **III-1** and **III-2**, respectively) < $F_2Mg\cdots C(CH_3)_3$ (15.56 kcal mol^{-1}). This trend also applies to the MgH_2-based series. Obviously, the interaction energy of an $X_2Mg\cdots$alkyl complex becomes larger as more methyl substituents are involved in the alkyl radical. Note that the interaction energy of isomer **II-2** is 0.18 kcal mol^{-1} larger than that of **II-1**, which might be attributed to the additional $F2^{\delta-}\cdots H2^{\delta+}$ interaction in **II-2**. Similarly, isomer **III-2** contains one more $F^{\delta-}\cdots H^{\delta+}$ secondary interaction compared with **III-1**, justifying its slightly larger interaction energy.

From Table 4, the interaction energies vary from −8.61 to −15.56 kcal mol^{-1} for the $F_2Mg\cdots Y$ complexes, and from −5.25 to −9.55 kcal mol^{-1} for the $H_2Mg\cdots Y$ series. Note that these values are comparable to those (−6.13 to −14.92 kcal mol^{-1})[58] of the $X_2Be\cdots Y$ [X = F, H; Y = CH_3, CH_2CH_3, $CH(CH_3)_2$, and $C(CH_3)_3$] complexes. Meanwhile, the interaction energies are −13.47 ∼ −15.80 kcal mol^{-1} for $F_2Mg\cdots\pi$ and −7.22 ∼ −8.91 kcal mol^{-1} for $H_2Mg\cdots\pi$ interactions where the π electron donors are acetylene, ethylene and benzene molecules.[36] Hence, it can be concluded that single-electron magnesium bond, single-electron beryllium bond, and π-magnesium bond are comparable in strength.

To deepen the understanding of the nature of single-electron Mg bond, the interaction energies of the $X_2Mg\cdots Y$ complexes have been further analyzed by using the LMOEDA method. The energy decomposition results present considerable electrostatic and polarization interactions in the complexation between MgX_2 and radical molecules. The former accounts for approximately half of the total attractive interaction energy, and the latter makes up 27.6–38.1% (see Table 5). Besides, the dispersion energy contributes 5.7–21.6% to the stabilization of the studied complexes, especially for the MgH_2-based series. From the table, all the terms, namely the electrostatic, polarization, exchange-repulsion and dispersion energies, increase with the growth of number of methyl groups in the system except that **III-2** has a slightly higher electrostatic energy than **IV**. The LMOEDA analysis also reveals that a $F_2Mg\cdots Y$ complex possesses larger attractive interaction energy and smaller

Table 4 BSSE-corrected interaction energies (in kcal mol^{-1}) and electron correlation effect (EC = [CCSD(T)-SCF]/CCSD(T) × 100%) of the $X_2Mg\cdots Y$ [X = F, H; Y = CH_3, CH_2CH_3, $CH(CH_3)_2$, $C(CH_3)_3$] complexes. The electron density (ρ, in au.) and its Laplacian ($\nabla^2\rho$, in au.) at the Mg⋯C1 BCP at the MP2/aug-*cc*-pVTZ level

	SCF	MP2	CCSD(T)	BSSE	EC	$\rho(r)$	$\nabla^2\rho(r)$
I	−7.34	−8.18	−8.61	0.54	14.8%	0.014	0.060
II-1	−9.21	−11.05	−11.52	0.89	20.1%	0.017	0.073
II-2	−9.48	−11.18	−11.70	0.81	19.0%	0.016	0.071
III-1	−10.53	−13.33	−13.81	1.21	23.8%	0.018	0.080
III-2	−10.90	−13.52	−14.06	1.09	22.5%	0.018	0.078
IV	−11.36	−15.12	−15.56	1.51	27.0%	0.019	0.084
I′	−2.71	−4.93	−5.25	0.19	48.4%	0.012	0.039
II′	−3.62	−6.94	−7.13	0.30	49.2%	0.013	0.048
III′	−4.12	−8.53	−8.60	0.41	52.1%	0.015	0.054
IV′	−4.05	−9.23	−9.55	0.52	57.6%	0.015	0.054

Table 5 LMOEDA partition terms (in kcal mol^{-1}) and the percentage contribution of electrostatic, polarization and dispersion components to the total attractive interaction energy for the $X_2Mg\cdots Y$ [X = F, H; Y = CH_3, CH_2CH_3, $CH(CH_3)_2$, $C(CH_3)_3$] complexes

	E_{elst}	E_{ex+rep}	E_{pol}	E_{disp}
I	−8.73 (57.8%)	6.95	−5.51 (36.5%)	−0.86 (5.7%)
II-1	−11.52 (54.2%)	10.17	−7.86 (37.0%)	−1.86 (8.8%)
II-2	−12.26 (56.6%)	10.73	−7.66 (35.4%)	−1.73 (8.0%)
III-1	−12.98 (51.3%)	11.94	−9.48 (37.5%)	−2.82 (11.2%)
III-2	−14.02 (54.5%)	12.20	−9.07 (35.3%)	−2.63 (10.2%)
IV	−13.92 (48.7%)	13.48	−10.90 (38.1%)	−3.78 (13.2%)
I′	−8.32 (55.8%)	9.95	−4.36 (29.3%)	−2.22 (14.9%)
II′	−10.50 (54.3%)	12.37	−5.50 (28.5%)	−3.33 (17.2%)
III′	−12.23 (53.0%)	14.51	−6.42 (27.8%)	−4.42 (19.2%)
IV′	−13.10 (50.8%)	16.14	−7.11 (27.6%)	−5.58 (21.6%)

Table 6 Main harmonic vibrational frequencies [ν (cm^{-1})] and corresponding infrared intensity of the $X_2Mg\cdots Y$ [X = F, H; Y = CH_3, CH_2CH_3, $CH(CH_3)_2$, $C(CH_3)_3$] complexes at the MP2/aug-*cc*-pVTZ level (the X-Mg-X symmetric stretching frequencies are 551.5 cm^{-1} and 1636.2 cm^{-1} in the MgF_2 and MgH_2 monomers, respectively; the X-Mg-X antisymmetric stretching frequencies are 861.3 cm^{-1} and 1659.0 cm^{-1} in the MgF_2 and MgH_2 monomers, respectively)

	X–Mg–X sym. stretch			X–Mg–X antisym. stretch			
	ν in complex	$\Delta\nu$	IR intensity	ν in complex	$\Delta\nu$	IR intensity	Mg···C stretch ν
I	544.7	−6.8	17.4	830.6	−30.7	152.5	209.5
II-1	544.1	−7.4	24.5	825.0	−36.3	96.0	229.2
II-2	543.6	−7.9	25.0	822.4	−38.9	146.5	224.5
III-1	542.5	−9.0	31.5	815.7	−45.6	140.3	258.5
III-2	543.2	−8.3	32.1	815.5	−45.8	142.5	249.7
IV	541.7	−9.8	34.2	809.9	−51.4	134.4	200.8
I′	1601.9	−34.3	13.4	1621.0	−38.0	484.3	150.4
II′	1594.7	−41.5	21.7	1612.5	−46.5	485.3	175.3
III′	1588.7	−47.5	33.6	1606.5	−52.5	473.0	231.9
IV′	1586.1	−50.1	38.1	1602.7	−56.3	465.6	352.8

exchange-repulsion energy than corresponding $H_2Mg\cdots Y$ complex, giving rise to the larger E_{int} value of the former.

3.3 Harmonic vibrational frequencies

Main harmonic vibrational frequencies and their corresponding infrared intensities of the $X_2Mg\cdots Y$ complexes are shown in Table 6. From the table, the magnesium bond stretching vibration of the $F_2Mg\cdots Y$ complexes occurs in the 200.8–258.5 cm^{-1} region, comparable to that of 208.0–240.7 cm^{-1} for the $F_2Mg\cdots\pi$ bonding species.[36] The Mg···C1 stretching vibrational frequency of the $H_2Mg\cdots Y$ series, on the other hand, shows an apparent increase as more methyl groups are involved in the electron donor.

From Table 6, both X–Mg–X symmetric and antisymmetric stretching vibrational frequencies decrease as a result of the complexation between MgX_2 and radical molecules, which accords well with the lengthening of the Mg–X bonds. The antisymmetric X–Mg–X and symmetric H–Mg–H stretching vibration frequencies are red-shifted by 30.7 to 56.3 cm^{-1} in the complexes. In contrast, the F–Mg–F symmetric stretching frequency has a minor redshift of less than 10 cm^{-1}. This may be attributed to the stronger intermolecular interaction of the $F_2Mg\cdots Y$ complexes and the bent structure of the MgF_2 subunit, which bring about coupling of the symmetric stretch of the F–Mg–F bond with the stretching Mg···C1 bond. Note that the similar vibrational-mode coupling even results in abnormal blue-shifted F–Be–F symmetric stretch in the studies of beryllium bonding systems.[34,58] In addition, it has been found that the antisymmetric stretching vibration of the MgX_2 subunit has larger IR intensity than symmetric stretching vibration, especially in the MgH_2-based complexes.

3.4 AIM analysis

Bader's quantum theory of atoms in molecules (QTAIM) was applied to the topic complexes to gain more insight into the nature of single-electron magnesium bond. The electron

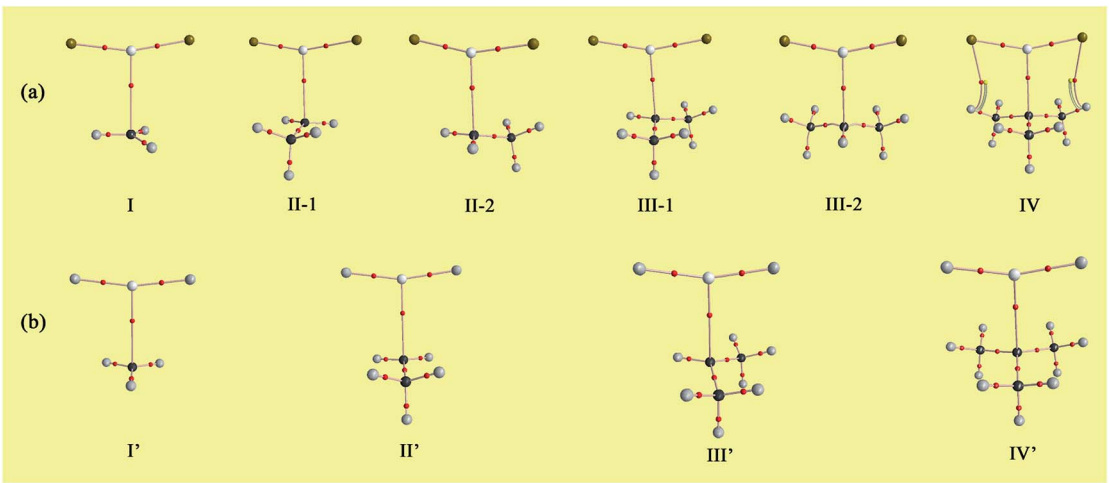

Fig. 4 Molecular graphs of the (a) $F_2Mg\cdots Y$ and (b) $H_2Mg\cdots Y$ [Y = CH_3, CH_2CH_3, $CH(CH_3)_2$, $C(CH_3)_3$] complexes.

densities (ρ) and their Laplacians ($\nabla^2\rho$) at the Mg···C1 bond critical points (BCPs) have been obtained, which are listed in Table 4. The molecular graphs of the complexes are presented in Fig. 4.

From Fig. 4, there are bond critical points between MgX_2 and radicals in all the cases, indicating the formation of single-electron magnesium bond therein. It is worth mentioning that there are also interaction paths between F of MgF_2 and H of the $C(CH_3)_3$ radical in complex **IV**, only their corresponding electron density ($\rho = 0.006$ au.) is quite small. As shown in Table 4, the values of electron density and Laplacians at the Mg···C1 BCPs are in the range of 0.012–0.019 and 0.039–0.084 au, respectively. Besides, both ρ and $\nabla^2\rho$ values increase gradually with the increasing number of methyl groups involved in the $X_2Mg\cdots Y$ complexes. From Fig. S3b,† the evolution of electron density at the Mg···C1 BCP shows a similar trend to that of interaction energy. This again reflects the positive role of the methyl substituent in the single-electron magnesium bond formation. According to a previous study of π-magnesium bond, the values of electron density at the $\pi\cdots$Mg BCPs also range from 0.012 to 0.019 au.,[36] also reflecting that π-magnesium bond and single-electron magnesium bond are close to each other in strength.

4. Conclusions

According to quantum chemical calculations, the MgX_2 (X = F, H) molecules are able to serve as Lewis acids and form complexes with alkyl radicals Y [Y = CH_3, CH_2CH_3, $CH(CH_3)_2$, and $C(CH_3)_3$]. The existence of single-electron magnesium bond is thereby proposed. Upon the interaction with radicals, the MgX_2 molecule becomes bent, accompanied by elongated Mg–X bonds and red-shifted X–Mg–X stretching vibrations. LMOEDA analysis demonstrates that the electrostatic and polarization interactions make dominant contributions to the stability of the topic complexes. Besides, there is 0.003–0.019$|e|$ electron transfer from the radical molecules to MgX_2 during complexation and the main electron donation takes place from the SOMO orbital of the radicals to the 3s or 3p orbital of Mg. It has been found that, the more methyl groups are involved in electron donor Y, the shorter the binding distance and the larger the interaction energy of the $X_2Mg\cdots Y$ complex, showing the positive effect of methyl substitution on single-electron magnesium bonding formation. We hope that the results of this study can further enrich the knowledge of intermolecular weak interactions, and may provide meaningful references for biological and chemical processes that involve radicals.

Conflicts of interest

There are no conflicts to declare.

Acknowledgements

This work was supported by the National Natural Science Foundation of China (Grant No. 21573089, 51872057) and the "13th Five-Year" Science and Technology Research Project of Jilin provincial education department (JJKH20190117KJ).

Notes and references

1 R. W. Saalfrank, H. Maid and A. Scheurer, *Angew. Chem., Int. Ed.*, 2008, **47**, 8794–8824.
2 A. Llanes-Pallas, C.-A. Palma, L. Piot, A. Belbakra, A. Listorti, M. Prato, P. Samorì, N. Armaroli and D. Bonifazi, *J. Am. Chem. Soc.*, 2009, **131**, 509–520.
3 A. Priimagi, G. Cavallo, P. Metrangolo and G. Resnati, *Acc. Chem. Res.*, 2013, **46**, 2686–2695.
4 A. Bauzá and A. Frontera, *Angew. Chem., Int. Ed.*, 2015, **54**, 7340–7343.
5 P. Politzer, J. S. Murray and T. Clark, *J. Mol. Model.*, 2015, **21**, 52.
6 G. Jones, P. Willett and R. C. Glen, *J. Mol. Biol.*, 1995, **245**, 43–53.
7 M. G. Chudzinski, C. A. McClary and M. S. Taylor, *J. Am. Chem. Soc.*, 2011, **133**, 10559–10567.
8 J. Itskovitz-Eldor, M. Schuldiner, D. Karsenti, A. Eden, O. Yanuka, M. Amit, H. Soreq and N. Benvenisty, *Mol. Med.*, 2000, **6**, 88–95.
9 R. B. Walsh, C. W. Padgett, P. Metrangolo, G. Resnati, T. W. Hanks and W. T. Pennington, *Cryst. Growth Des.*, 2001, **1**, 165–175.
10 V. N. Lindsay, C. Nicolas and A. B. Charette, *J. Am. Chem. Soc.*, 2011, **133**, 8972–8981.
11 P.-P. Zhou and W.-Y. Qiu, *J. Phys. Chem. A*, 2009, **113**, 10306–10320.
12 A. Laguna, T. Lasanta, J. M. López-de-Luzuriaga, M. Monge, P. Naumov and M. E. Olmos, *J. Am. Chem. Soc.*, 2010, **132**, 456–457.
13 J. Lieffrig, H. M. Yamamoto, T. Kusamoto, H. Cui, O. Jeannin, M. Fourmigué and R. Kato, *Cryst. Growth Des.*, 2011, **11**, 4267–4271.
14 N. Sakai, J. Mareda and S. Matile, *Acc. Chem. Res.*, 2005, **38**, 79–87.
15 Q. Li, Q. Lin, W. Li, J. Cheng, B. Gong and J. Sun, *ChemPhysChem*, 2008, **9**, 2265–2269.
16 A. Ebrahimi, M. Habibi, R. S. Neyband and A. R. Gholipour, *Phys. Chem. Chem. Phys.*, 2009, **11**, 11424–11431.
17 J. K. Khedkar, M. M. Deshmukh, S. R. Gadre and S. P. Gejji, *J. Phys. Chem. A*, 2012, **116**, 3739–3744.
18 E. Rossi, M. De Santis, D. Sorbelli, L. Storchi, L. Belpassi and P. Belanzoni, *Phys. Chem. Chem. Phys.*, 2020, **22**, 1897–1910.
19 P. R. Varadwaj, A. Varadwaj and H. M. Marques, *Inorganics*, 2019, **7**, 40.
20 P. R. Varadwaj, *Molecules*, 2019, **24**, 3166.
21 Y. Nishiyama, P. Langan and H. Chanzy, *J. Am. Chem. Soc.*, 2002, **124**, 9074–9082.
22 Y. Nishiyama, J. Sugiyama, H. Chanzy and P. Langan, *J. Am. Chem. Soc.*, 2003, **125**, 14300–14306.
23 K. P. Gierszal, J. G. Davis, M. D. Hands, D. S. Wilcox, L. V. Slipchenko and D. Ben-Amotz, *J. Phys. Chem. Lett.*, 2011, **2**, 2930–2933.

24 A. Bajpai, M. Lusi and M. J. Zaworotko, *Chem. Commun.*, 2017, **53**, 3978–3981.
25 B.-Q. Wang, Z.-R. Li, D. Wu, X.-Y. Hao, R.-J. Li and C.-C. Sun, *Chem. Phys. Lett.*, 2003, **375**, 91–95.
26 H. Cybulski, E. Tymińska and J. Sadlej, *ChemPhysChem*, 2006, **7**, 629–639.
27 X.-Y. Hao, Z.-R. Li, D. Wu, Z.-S. Li and C.-C. Sun, *J. Chem. Phys.*, 2003, **118**, 10939–10943.
28 T. Tsurusawa and S. Iwata, *J. Chem. Phys.*, 2000, **112**, 5705–5710.
29 Y. Li, D. Wu, Z.-R. Li, W. Chen and C.-C. Sun, *J. Chem. Phys.*, 2006, **125**, 084317.
30 K. Yuan, Y.-Z. Liu, L.-L. LÜ, Y.-C. Zhu, J. Zhang and J.-Y. Zhang, *Chin. J. Chem.*, 2009, **27**, 697–702.
31 Q. Li, Y. Wang, W. Li, J. Cheng, B. Gong and J. Sun, *Phys. Chem. Chem. Phys.*, 2009, **11**, 2402–2407.
32 Z.-F. Li, Y.-C. Zhu and H.-X. Li, *Phys. Chem. Chem. Phys.*, 2009, **11**, 11113–11120.
33 Z. Li, X. Zhang, H. Li, Y. Zhu and X. Yang, *Chem. Phys. Lett.*, 2011, **510**, 273–277.
34 M. Yáñez, P. Sanz, O. Mó, I. Alkorta and J. Elguero, *J. Chem. Theory Comput.*, 2009, **5**, 2763–2771.
35 X. Yang, Q. Li, J. Cheng and W. Li, *J. Mol. Model.*, 2013, **19**, 247–253.
36 S.-Y. Li, D. Wu, Y. Li, D. Yu, J.-Y. Liu and Z.-R. Li, *RSC Adv.*, 2016, **6**, 102754–102761.
37 C.-Y. Li, E. A. Hemmig, J. Kong, J. Yoo, S. Hernández-Ainsa, U. F. Keyser and A. Aksimentiev, *ACS Nano*, 2015, **9**, 1420–1433.
38 E. P. Gates, J. K. Jensen, J. N. Harb and A. T. Woolley, *RSC Adv.*, 2015, **5**, 8134–8141.
39 J. W. Tucker, J. D. Nguyen, J. M. Narayanam, S. W. Krabbe and C. R. Stephenson, *Chem. Commun.*, 2010, **46**, 4985–4987.
40 H. G. Yayla and R. R. Knowles, *Synlett*, 2014, **25**, 2819–2826.
41 F. Hasager, S. T. Andersen, S. A. Hass, M. P. Sulbaek Andersen and O. J. Nielsen, *J. Phys. Chem. A*, 2019, **123**, 10315–10322.
42 A. M. Arangio, H. Tong, J. Socorro, U. Poschl and M. Shiraiwa, *Atmos. Chem. Phys.*, 2016, **16**, 13105–13119.
43 C. Prescott and S. E. Bottle, *Cell Biochem. Biophys.*, 2017, **75**, 227–240.
44 V. Marchand, N. Charlier, J. Verrax, P. Buc-Calderon, P. Levêque and B. Gallez, *PLoS One*, 2017, **12**, e0172998.
45 S. F. Boys and F. Bernardi, *Mol. Phys.*, 1970, **19**, 553–566.
46 J. E. Carpenter and F. Weinhold, *J. Mol. Struct.: THEOCHEM*, 1988, **169**, 41–62.
47 M. J. Frisch, G. Trucks, H. Schlegel, G. Scuseria, M. Robb, J. Cheeseman, G. Scalmani, V. Barone, B. Mennucci and G. Petersson, *Gaussian 09*, Gaussian Inc., Wallingford, CT, 2009.
48 R. F. W. Bader and C. F. Matta, *J. Phys. Chem. A*, 2004, **108**, 8385–8394.
49 F. Cortés-Guzmán and R. F. W. Bader, *Coord. Chem. Rev.*, 2005, **249**, 633–662.
50 E. R. Johnson, S. Keinan, P. Mori-Sánchez, J. Contreras-García, A. J. Cohen and W. Yang, *J. Am. Chem. Soc.*, 2010, **132**, 6498–6506.
51 T. Lu and F. Chen, *J. Comput. Chem.*, 2012, **33**, 580–592.
52 C. Lefebvre, G. Rubez, H. Khartabil, J.-C. Boisson, J. Contreras-García and E. Hénon, *Phys. Chem. Chem. Phys.*, 2017, **19**, 17928–17936.
53 W. Humphrey, A. Dalke and K. Schulten, *J. Mol. Graphics*, 1996, **14**, 33–38.
54 S. F. Boys and F. d. Bernardi, *Mol. Phys.*, 1970, **19**, 553–566.
55 P. Su and H. Li, *J. Chem. Phys.*, 2009, **131**, 014102.
56 M. W. Schmidt, K. K. Baldridge, J. A. Boatz, S. T. Elbert, M. S. Gordon, J. H. Jensen, S. Koseki, N. Matsunaga, K. A. Nguyen and S. Su, *J. Comput. Chem.*, 1993, **14**, 1347–1363.
57 S. S. Batsanov, *Inorg. Mater.*, 2001, **37**, 871–885.
58 D. Yu, D. Wu, Y. Li and S.-Y. Li, *Theor. Chem. Acc.*, 2016, **135**, 112.